Dual metal hydride hydrogen storage system with thermal coupling for enhanced refueling processes

Giovanni Di Ilio [a], Sohaib Raza [b], Gabriele Scarpati [c], Elio Jannelli [d]

[a] University of Naples "Parthenope", Naples, Italy, giovanni.diilio@uniparthenope.it
[b] University of Naples "Parthenope", Naples, Italy, sohaib.raza001@studenti.uniparthenope.it
[c] Helmholtz-Zentrum HEREON GmbH, Geesthacht, Germany, gabriele.scarpati@hereon.de
[d] University of Naples "Parthenope", Naples, Italy, elio.jannelli@uniparthenope.it

Abstract:

The implementation of metal hydride-based hydrogen storage systems offers an interesting alternative to high-pressure gas and liquid storage, thanks to their higher volumetric storage capacity and the possibility of designing tanks with a flexible and convenient layout. In this work, a metal hydride hydrogen storage system is investigated, where a source tank supplies hydrogen to a receiver tank to be refueled. The source storage is designed in a modular configuration, consisting of one or multiple identical modules, each equivalent to the receiver tank. The two storages are connected to each other via a heat transfer medium, in a way to exploit the endo/exo-thermic reactions occurring during the process and realize an integrated thermal management of the two metal hydride tank systems. The underlying principle is that the heat produced by the hydrogen absorption process in the receiver tank is released to the material contained in the source storage, which instead requires heat to promote the hydrogen desorption reaction. The hydrogen release process is driven by the pressure difference between the equilibrium pressure of the metal hydride in the two systems, which in turn depends on the temperature conditions. A parametric analysis is conducted by varying the size of the source tank system, achieved by changing the number of identical modules composing it. Moreover, different aspect ratios are considered for the base tank design, to identify the most suitable configuration and operating conditions that ensure fast refueling of the receiver tank. The results show the effectiveness of the investigated approach, and provide insights into the system's performance in achieving fast and energy-efficient hydrogen transfer under different layouts and working conditions. The integrated thermal management leads to an optimal exploitation of the heat released by the receiver tank and absorbed by the source storage system. The approach presented in this work retains the advantages of metal hydrides, as it operates at mild pressure and temperature conditions (which is preferential both for safety and energy reasons), while overcoming their main limitation, related to the management of the heat involved in the absorption/desorption process.

Keywords:

Metal Hydrides; Hydrogen Storage; Thermal Management; Numerical Modelling.

1. Introduction

The urgent need to mitigate climate change while simultaneously addressing the continuous growth in global energy demand is driving the transition toward sustainable energy technologies. In this context, green hydrogen, produced using renewable energy sources such as solar and wind power plants, has emerged as a key option. This versatile energy carrier can be utilized across a wide range of applications, including power generation for residential and industrial sectors, fuel for transportation, and various industrial processes **[1]**, which in turn motivates the development of efficient storage methods. In fact, hydrogen can be stored in three primary ways: as a high-pressure gas, as a liquefied fluid, or within solid-state materials **[2]**, each with its own advantages and limitations. High-pressure gaseous hydrogen storage is a mature technology, which enables rapid hydrogen charging and discharging but suffers from high cost, safety concerns, and low volumetric energy density **[3]**. Liquid hydrogen technology instead, better meets storage practical requirements in terms of both mass and volumetric density, yet it presents several critical challenges, including high energy consumption, boil-off issues and high cost **[4]**. Low-pressure hydrogen storage via metal hydrides (MHs), on the other hand, offers a less common but interesting alternative, with distinct advantages and drawbacks that are here briefly recalled. The key aspect of this approach lies in the possibility to operate under mild pressure and temperature conditions, thereby mitigating the safety, technical and economic challenges associated with high-pressure and low-temperature storages **[5-8]**. Moreover, MHs provide high volumetric energy density, enabling the design of compact tanks with optimized shapes that can efficiently accommodate hydrogen storage within very limited space. However, MHs also present significant challenges due to the heat effects associated with their reversible hydrogen reactions. During hydrogen absorption (hydrogenation), the exothermic formation of the hydride releases substantial amounts of heat, while hydrogen desorption (dehydrogenation) is endothermic and requires an external heat supply to release the stored hydrogen. The

poor thermal conductivity of the hydride bed poses an additional challenge, as it hinders efficient heat distribution throughout the material. Consequently, effective hydrogen storage with MHs demands advanced thermal management systems capable of handling high thermal fluxes and maintaining efficient operation. The thermal management issue of MH tanks has been widely explored in the literature, with several different strategies proposed to efficiently control the heat generated or required, depending on the specific application **[9]**. Broadly, these strategies can be grouped into heat exchanger-based and thermochemical approaches. Heat exchanger solutions are further classified as internal or external, depending on whether the thermal fluid is circulated inside or around the tank **[10-14]**. Internal designs often include axially arranged tubes, coiled tubes, mini-channels, or finned reactors, which improve radial temperature uniformity and conduction within the MH bed while minimizing reductions in volumetric storage capacity. External solutions, such as fins, tubes, or cooling jackets attached to the tank surface, are effective but typically reduce volumetric efficiency more than internal configurations. Integration with fuel cells represents a special case of thermal management, where waste heat from the cell can support the endothermic desorption process, particularly in vehicular applications **[15-17]**. Thermochemical strategies complement these approaches by exploiting phase change materials (PCMs) or reversible chemical reactions to absorb or supply heat during hydrogen cycling **[18,19]**. Engineered layouts, such as honeycomb or layered geometries, are typically employed to enhance heat conduction in PCM-based systems. Additionally, coupling MH tanks with batteries has been investigated, allowing the heat generated by battery operation to facilitate hydrogen desorption **[20-24]**.

As an extension of conventional thermal management strategies for MH tanks, thermally coupling a receiver tank with a donor storage system offers a way to enhance hydrogen transfer efficiency. In this configuration, the exothermic heat released during hydrogen absorption in the receiver tank (potentially the MH tank of a hydrogen-powered vehicle) is transferred to the donor tank (which can correspond to the stationary tank of a hydrogen refueling station) to drive the endothermic desorption process, thereby reducing the need for external energy inputs. Therefore, exploiting this internal heat exchange can significantly improve the energy efficiency of the entire hydrogen storage system, suggesting its potential to enhance the sustainability and performance of hydrogen mobility scenarios.

This concept is investigated in this study, where, to quantify the thermal coupling effect, a parametric analysis is conducted on a representative MH storage system in which a heat transfer fluid (i.e. water) circulate between the receiver and donor tanks, providing the exchange of thermal energy and supporting both hydrogenation and dehydrogenation reactions. The analysis is carried out using a 2D axisymmetric finite element method (FEM) to accurately capture the heat transfer phenomena within the coupled MH tanks. To assess the influence of system design on thermal performance, the study systematically varies the size of the source storage system by changing the number of modules it comprises, with each module identical to the receiver tank. In addition, the geometry of the base tank is parametrically modified by varying its aspect ratio, enabling the evaluation of a wide range of possible layouts and operating conditions. The impact of the heat transfer fluid (HTF) flow rate is also examined to understand its role in enhancing thermal coupling between the tanks. Through this comprehensive parametric approach, the study aims to highlight how internal heat recovery can be effectively leveraged to support hydrogen absorption and desorption processes, providing detailed insights into strategies for improving both the speed and energy efficiency of hydrogen refueling operations in MH systems.

2. Materials and methods

2.1 Coupled MH tanks system description and operation

The considered system consists of a receiver tank coupled with a modular source storage system composed of multiple identical MH tanks connected in parallel. The adoption of a multi-tank source configuration allows the overall storage capacity of the source system to exceed that of the receiver tank, reflecting typical operating conditions in hydrogen refueling scenarios, such as the interaction between a refueling station and a vehicle. In addition, this configuration enables the source system to potentially supply multiple receiver tanks in sequence, as only a fraction of the stored hydrogen is extracted from each module during a single refueling process.

Each tank of the coupled system is designed as a hollow cylindrical vessel characterized by a given aspect ratio, within which the HTF (i.e. water) flows axially, and all tanks are considered to be identical. The HTF operates in a closed-loop configuration, continuously circulating between the receiver and source tanks to enable thermal energy exchange during both hydrogen absorption and desorption phases. By this means, the exothermic heat generated during absorption can be efficiently utilized to meet the endothermic requirements of desorption. A schematic representation of the system is provided in Figure 1. Particular attention is given to the relative arrangement of hydrogen and HTF flow directions. In the receiver tank, the hydrogen inlet is aligned with the HTF inlet, as the region where hydrogen enters is associated with the highest heat generation due to the exothermic absorption reaction, thus requiring lower HTF temperatures for effective heat removal. Conversely, in the source tank, the HTF enters at the hydrogen outlet side, where higher temperatures are

needed to sustain the endothermic desorption process. Within this framework, the system operates by coupling the two sub-systems initially at different thermodynamic states: the receiver tank is initially nearly empty, this state corresponding to ambient temperature and pressure conditions, while the source tanks are fully charged, with hydrogen stored at an imposed nominal pressure (i.e. 30 bar) at ambient temperature. Once the connection between receiver and source tanks is enabled, gaseous hydrogen contained within the pore space rapidly redistributes. Hence, a global common gas pressure is established, leading to a pressure difference between this and the equilibrium pressure in each tank, which trigger the onset of hydrogen absorption and desorption processes. In particular, the initially depleted (receiver) tank experiences a gas pressure higher than its local absorption equilibrium pressure, thereby promoting hydrogen uptake. In contrast, the initially fully-charged (source) tanks operate at a pressure lower than their desorption equilibrium pressure, leading to hydrogen release. In this configuration, one tank effectively acts as a hydrogen sink, while the other behaves as a source, with the gaseous phase serving as an intermediate buffer. As the process evolves, the two sub-systems induce opposing effects (i.e. opposite pressure variations) on the gas phase. Hydrogen absorption in the receiver tank continuously removes gaseous hydrogen, tending to locally decrease the gas pressure, whereas desorption in the source tanks releases hydrogen, tending to increase it. However, since the two sub-systems are directly connected, pressure equalization in the gas phase is assumed to be instantaneous. As a consequence, no sustained pressure gradient can exist between the tanks, and the system always evolves under a common, global gas pressure. Moreover, because the driving force for absorption and desorption is kinetic in nature, and depends mainly on the pressure difference between the actual gas pressure and the local equilibrium pressure in each tank, the absorption and desorption rates are generally not symmetric. A larger deviation between the gas pressure and the corresponding equilibrium pressure results in a faster reaction rate. As a result, although the pressure may exhibit a transient overshoot or undershoot during the early stages of the process, it progressively evolves toward a global equilibrium pressure. This final pressure corresponds to the condition where the net hydrogen transfer between the two solid phases vanishes because neither absorption nor desorption is possible anymore.

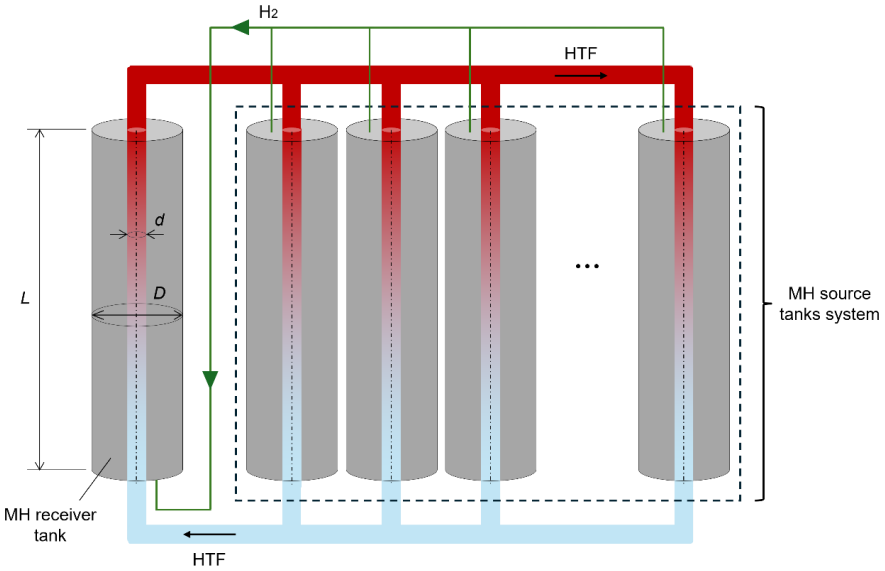

Figure 1. Schematic representation of the couple MH tanks system.

The MH material selected for this study is the Hydralloy C5, a commercial AB_2-type alloy **[25]**, which is employed in all tanks. This material has been chosen for its operational flexibility over a wide range of temperature and pressure, near ambient conditions. Each individual tank, whose aspect ratio is varied as described in the following sections, has a nominal hydrogen storage capacity of approximately 53 g, calculated at reference conditions of 30 bar and 20 °C by accounting for both the hydrogen that can be absorbed in the solid phase (i.e. 51.4 g) and the hydrogen present in the gaseous phase (i.e. 1.3 g). The main characteristics of the base tank are summarized in Table 1.

Table 1. Base-tank main characteristics.

Parameter	**Value**
Nominal H2 storage capacity	53 g
Mass of MH material	2.8 kg
Absorption plateau pressure at 20 °C	~ 10-11 bar
Desorption plateau pressure at 20 °C	~ 6-7 bar
Absorption enthalpy (ΔH_{abs})	22.3 kJ/mol
Desorption enthalpy (ΔH_{des})	28.4 kJ/mol

2.2 Numerical modelling approach

The numerical model used in this work is a 2D axisymmetric FEM developed in COMSOL Multiphysics, which allows to simulate the coupled absorption and desorption processes occurring in the system. The model considers the MH material as a porous medium, with the mass transport of hydrogen accounted for by the Darcy's law. The HTF instead is modelled using the Reynolds–Averaged Navier–Stokes (RANS) turbulence approach.

2.2.1 MH model

The governing equations of the MH model are summarized below, while a detailed formulation can be found in **[11]**. The adopted MH model relies on the following assumptions: i) the MH particles are assumed to expand linearly with increasing hydrogen concentration; ii) a finite contact area exists between neighbouring particles; iii) particles are approximated as quasi-spherical; iv) the gaseous hydrogen is in thermal equilibrium with the solid matrix; v) heat conduction occurs through three parallel paths: the gas region, the biphasic region, and the solid particles; vi) radiative heat transfer is considered negligible; vii) the MH properties vary with hydrogen concentration, transitioning from pure alloy to pure hydride, except for the specific heat capacity, which is assumed constant and equal to that of the metal alloy. The MH bed is described by a mass conservation equation for hydrogen in the gaseous phase and an energy conservation equation to capture the system behavior during absorption and desorption processes. A real gas equation of state is also employed to account for the non-ideal behavior of hydrogen. The mass conservation is given by:

$$\frac{\partial\left(\varepsilon\rho_{H_2}\right)}{\partial t}+\nabla\cdot\left(\rho_{H_2}\boldsymbol{u_{H_2}}\right)+\nu_H M_H=0 \tag{1}$$

where $\rho_{H_2}=f(P,T)$ is the density of hydrogen in gaseous phase, M_H is the atomic hydrogen molar mass, ν_H is the atomic hydrogen reaction rate, ε is the porosity, and $\boldsymbol{u_{H_2}}$ is the velocity of the hydrogen flow, which is expressed through the Darcy's law, as follows:

$$\boldsymbol{u_{H_2}}=-\frac{\kappa}{\mu_{H_2}}\nabla P \tag{2}$$

In Eq. 2, P is the pressure, κ is the permeability in the porous media and $\mu_{H_2}=f(P,T)$ is the dynamic viscosity of hydrogen. The energy conservation is expressed by the following equation:

$$\left(\rho c_p\right)_{eff}\frac{\partial T}{\partial t}+\rho_{H_2}c_{p,H_2}\boldsymbol{u_{H_2}}\cdot\nabla T=\nabla\cdot\left(k_{eff}\nabla T\right)+\dot{Q}_{react}+\dot{Q}_{gas} \tag{3}$$

where T is the temperature, $c_{p,H_2}=f(P,T)$ is the hydrogen specific heat at constant pressure, k_{eff} is the effective thermal conductivity, while $\dot{Q}_{react}=-\nu_H\,\Delta H/2$ and $\dot{Q}_{gas}=\varepsilon\,\partial p/\partial t$ are the heat source related to the hydrogenation or dehydrogenation reaction, and the gas pressure-volume power during expansion/compression, respectively. The term $\left(\rho c_p\right)_{eff}$ in Eq. 3 represents the effective volumetric heat capacity and it is calculated as:

$$\left(\rho c_p\right)_{eff}=\varepsilon\rho_{H_2}c_{p,H_2}+(1-\varepsilon)\rho_{MH}c_{p,MH} \tag{4}$$

where $c_{p,MH}=500\ \mathrm{J/kgK}$ is the specific heat capacity of the MH solid matrix, and ρ_{MH} is the density of the MH, defined as the ratio between the MH mass m_{MH} and its volume V_{MH}:

$$\rho_{MH}=\frac{m_{MH}}{V_{MH}} \tag{5}$$

The MH mass is given by the sum of the hydrogen mass (m_{H_2}) and the mass of the metal alloy (m_{met}), that is:

$$m_{MH}=m_{H_2}+m_{met}=\frac{1}{1-X}m_{met} \tag{6}$$

while V_{MH} is related to the metal alloy volume (V_{met}) through the maximum MH expansion factor, namely $Exp_{MH,max}=21.34\%$ **[26]**, as follows:

$$V_{MH}=V_{met}\left(1+F\cdot Exp_{MH,max}\right) \tag{7}$$

In Eqs. 6 and 7, the hydrogen concentration X and the reacted fraction F have been introduced, which are defined as follows, respectively;

$$X=\frac{m_{H_2}}{m_{MH}}\quad;\quad F=\frac{X}{X_{max}} \tag{8}$$

where $X_{max} \cong 1.8$ wt% for the Hydralloy C5. The true density of the metal alloy ($\rho_{met,t} = m_{met}/V_{met}$) is taken equal to $6380\ kg/m^3$ according to **[26]**, while its bulk density for the non-reacted material ($\rho_{met,bulk,0}$) has been assumed equal to $3000\ kg/m^3$. As far as the kinetic modeling is concerned, the hydrogen reaction is described using a specific expression for the Hydralloy C5 **[27,28]**:

$$\nu_H = \frac{m_{met}}{V_{bulk} M_H} K_0 \cdot e^{-\frac{E_a}{RT}} \cdot \frac{P - P_{eq}}{P_{eq}} \cdot \left(X - X_{eq}\right) \tag{9}$$

where $K_0 = 5.85 \cdot 10^6\ s^{-1}$ is the pre-exponential factor, $E_a = 40\ kJ/mol_{H_2}$ is the activation energy, R is the gas constant, and P_{eq} and X_{eq} are the equilibrium pressure and the equilibrium hydrogen concentration **[11,29]**, respectively. The term V_{bulk} in Eq. 9 represents the total volume of the considered system, corresponding to the difference between V_{tank} and V_{free}, the former being the whole tank volume, and the latter being the (variable) volume which is not occupied by the porous material. The equation suggested by Dunikov et al. **[30]** was used for the porosity:

$$\varepsilon = \varepsilon_0 \frac{1 - \frac{1}{\varepsilon_0} F \cdot \delta\rho}{1 - F \cdot \delta\rho} \tag{10}$$

where ε_0 is the porosity for $F = 0$, given by:

$$\varepsilon_0 = 1 - \frac{\rho_{met,bulk,0}}{\rho_{met,t}} \tag{11}$$

and $\delta\rho$ is calculated as:

$$\delta\rho = \frac{\rho_{met,t} - \rho_{MH,F=1}}{\rho_{met,t}} \tag{12}$$

In Eq. 12, the term $\rho_{MH,F=1}$ is the density of the MH (Eqs. 5-7) for $F = 1$. Regarding the permeability, a suitable model is required to describe the flow resistance through the porous MH bed. For this purpose, the Kozeny–Carman equation has been adopted:

$$\kappa = \frac{1}{180} \frac{\varepsilon^3 d_p^2}{(1-\varepsilon)^2} \tag{13}$$

where $d_p = f(F)$ **[26]** represents the particle diameter. The effective thermal conductivity k_{eff}, which is another key property of MH systems, is modelled through the modified Sun and Deng approach **[31]** where it is a function of the hydrogen thermal conductivity $k_{H_2} = f(P,T)$, the solid-phase thermal conductivity $k_s = f(F)$, the porosity and the contact angle between solid particles, $\theta = f(F)$.

2.2.2 HTF model

As far as the HTF is concerned (i.e. water), this is modeled as an incompressible fluid, with its flow field described using a RANS approach with a k–ε turbulence model. The thermal behavior of the HTF instead is described by the following energy conservation equation:

$$\rho_{HTF} c_{p,HTF} \frac{\partial T}{\partial t} + \rho_{HTF} c_{p,HTF} \boldsymbol{u} \cdot \nabla T = \nabla \cdot (k_{HTF} \nabla T) \tag{14}$$

where $\rho_{HTF} = f(T)$, $c_{p,HTF} = f(T)$ and $k_{HTF} = f(T)$ are the density, specific heat at constant pressure and thermal conductivity of the HTF, respectively, while $\boldsymbol{u}$ is the velocity filed. This formulation enables the evaluation of heat exchange between the HTF and the surrounding MH domain.

2.2.3 MH tanks coupling approach

As mentioned above, the source tanks are assumed to be identical and connected in parallel; therefore, only one representative tank is explicitly simulated. In this framework, both the hydrogen mass flow rate and the HTF flow rate are scaled accordingly, each representing a fraction of the total flow exchanged with the receiver tank. The coupling between the source (hereafter referred to as *desorption* tank, or DES tank) and receiver (hereafter referred to as *absorption* tank, or ABS tank) is then implemented through appropriate boundary conditions applied to both the MH and HTF sub-domains, ensuring a physically consistent interaction between the two sub-systems. In particular, as far as the MH domain is concerned, the coupling is enforced by prescribing a pressure boundary condition at the hydrogen outlet section of the source tank and a corresponding mass flux at the hydrogen inlet section of the receiver tank. In addition, in order to avoid non-physical discontinuities and also to mimic the gradual opening of the valve connecting the tanks at the beginning of the hydrogen transfer process, a time-dependent, physically coupled ramp is introduced.

Specifically, at the outlet of the source tank, the pressure is initially imposed as a function of time, transitioning smoothly from the initial pressure ($P_{\mathrm{des},0}$) to the instantaneous pressure at the receiver inlet. Once the two pressures become equal, the ramp is terminated and a fully coupled condition is established, whereby the outlet pressure of the source tank directly follows the inlet pressure of the receiver tank. The corresponding mathematical formulation of such a coupling boundary condition is the following:

$$\begin{cases} P_{des,out}(t) = P_{des,0} + \dfrac{t}{t_{ramp}}\left(P_{abs,in}(t) - P_{des,0}\right), & for\ t \le t_{ramp} \\ P_{des,out}(t) = P_{abs,in}(t), & for\ t > t_{ramp} \end{cases} \tag{15}$$

where subscripts *des* and *abs* refer to the source *desorption* tank and the receiver *absorption* tank, respectively, while subscripts *in* and *out* refer to the hydrogen inlet and outlet sections of the tanks, respectively. The parameter t_{ramp} in Eq. 15 represents the pressure ramp duration, which is determined through a sensitivity analysis, as discussed later. It is worth noting that, in order to avoid numerical instabilities, the hydrogen inlet and outlet sections are assumed to coincide with the entire circular cross-section of the tanks. On the receiver side, instead, the inlet hydrogen mass flow rate is imposed equal to the total hydrogen mass flow rate leaving the source system, evaluated at each time step, thereby ensuring strict mass conservation. This approach allows the system pressure to evolve naturally after the initial transient, governed solely by the kinetics of absorption and desorption and by the overall mass balance. Such a boundary condition reads as follows:

$$\dot{m}_{H_2,abs,in}(t) = n_{des}\dot{m}_{H_2,des,out}(t) \tag{16}$$

where n_{des} is the number of desorption tanks operating in parallel. Regarding the HTF domain, a closed-loop configuration is considered to enable continuous thermal coupling between the tanks. In particular, the same total mass flow rate of HTF is imposed throughout the system. Since the HTF channels in all tanks have identical cross-sectional areas, this condition can be equivalently expressed in terms of velocity. Accordingly, the (uniform) velocity imposed at the inlet of each desorption tank is defined as a fraction of the (uniform) inlet velocity at the receiver tank, that is:

$$u_{des,in}(t) = u_{abs,in}(t)/n_{des} \tag{17}$$

This condition ensures a consistent distribution of the HTF flow rate among the parallel modules of the source system. Furthermore, the thermal coupling is further enforced through temperature boundary conditions: the (uniform) HTF temperature at the inlet of each desorption tank is set equal to the cross-sectional average temperature at the outlet of the absorption tank; conversely, the (uniform) HTF temperature at the inlet of the absorption tank is imposed as the average outlet temperature of the desorption tanks, which are assumed to operate under identical conditions. This condition reads as follows:

$$T_{des,in}(t) = \bar{T}_{abs,out}(t) \quad , \quad T_{abs,in}(t) = \bar{T}_{des,out}(t) \tag{18}$$

where $\bar{T}$ represents the cross-sectional average temperature. This formulation ensures consistent heat exchange between the two sub-systems and enables the recovery of thermal energy within the loop.

2.3 Parametric case studies

A parametric analysis is carried out to investigate the effect of both system configuration and operating conditions on the thermal coupling and hydrogen transfer performance. The system always consists of a single absorption tank coupled with a modular source storage system composed of identical tanks connected in parallel. Accordingly, the number of desorption tanks is varied by considering 1, 20 and 50 tanks, thus effectively changing the capacity ratio (CR) between the source system and the receiver. At the same time, the geometry of the individual tank is modified by varying its aspect ratio (L/D), while maintaining a constant hydrogen storage capacity (see Table 1). The selected aspect ratios are 6.7, 18.6, and 33.7, corresponding to the geometrical parameters reported in Table 2, where all the analyzed cases are summarized. The diameter of the HTF channel instead is kept constant in all simulations and equal to 1 cm. In addition, a sensitivity analysis is performed on the pressure ramp duration t_{ramp}, which is varied between 1 and 10 s in order to assess its influence on the initial transient and overall system response. Finally, two representative values of the HTF velocity at the absorption tank inlet are also considered, equal to 0.1 m/s and 1 m/s, corresponding to volumetric flow rates of approximately 0.5 and 5 L/min, respectively. These two cases are selected to represent significantly different operating regimes, associated with slow and fast refueling conditions. In particular, they correspond to reference scenarios in which the full hydrogen capacity of the absorption tank is transferred within 50 minutes and 5 minutes, respectively. Under these assumptions, the reaction enthalpy associated with hydrogen absorption allows estimating the corresponding thermal power that must be theoretically removed in order to ideally keep the MH material at constant temperature (without accounting for

the thermal inertia of the MH material). This results in approximately 174 W for the slow refueling case and 1.74 kW for the faster one. By imposing a reference temperature difference of 5 °C between the HTF inlet and outlet in the absorption tank, and considering the specific heat capacity of the HTF, the required mass flow rate of the HTF, and consequently its volumetric flow rate and velocity, can be derived. It should be noted that this estimation is used only to define representative operating conditions, while the actual hydrogen transfer rates and HTF temperature differences naturally vary depending on the specific configuration and operating parameters considered in each case. The resulting Reynolds numbers are approximately 1058 and 10580 for the two cases, respectively. This indicates that the flow is in the laminar regime in the first case, while it becomes turbulent in the second, the latter ensuring more effective convective heat transfer between the HTF and the MH material.

Table 2. Parametric matrix defining the investigated system's configurations.

Case ID	CR	L/D	L [m]	D [cm]
1	1	6.7	0.4	6.0
2	20	6.7	0.4	6.0
3	50	6.7	0.4	6.0
4	1	18.6	0.8	4.3
5	20	18.6	0.8	4.3
6	50	18.6	0.8	4.3
7	1	33.7	1.2	3.6
8	20	33.7	1.2	3.6
9	50	33.7	1.2	3.6

The sensitivity analysis on the pressure ramp duration and HTF velocity is conducted only for the case with a single desorption tank and aspect ratio of 6.7 (i.e. Case #1 in Table 2).

2.4 Simulation setup

For all the investigated cases, the same initial conditions are adopted, as summarized in Table 3. In particular, the initial hydrogen concentration/reacted fraction in each tank is set consistently with the thermodynamic equilibrium corresponding to the imposed initial temperature and pressure conditions. Uniform fields are applied for all variables within each domain at the initial time.

Table 3. Initial conditions applied in all simulations.

Parameter	**ABS tank**	**DES tank**
Initial temperature [°C]	20	20
Initial pressure [bar]	1	30
Initial H_2 concentration [wt%]	0.147	1.80
Initial reacted fraction [%]	8.2	100

The HTF is also initially in thermal equilibrium with the tanks, i.e., at a uniform temperature of 20 °C, equal to that of the MH material. As far as the boundary conditions are concerned, each tank is assumed to be thermally insulated from the external environment, i.e., adiabatic boundary conditions are imposed at the outer walls. The remaining boundary conditions, which enable the coupling between the two sub-systems, have been outlined in previous sections. Finally, each simulation is carried out over a total duration of 30 minutes.

3. Results and discussion

The analysis begins with a sensitivity study on the pressure ramp duration and the HTF inlet velocity, carried out for the reference configuration consisting of a single desorption tank. The results of this preliminary investigation are used to define the final modeling setup adopted for all subsequent simulations. Once the reference conditions are established, the effects of the main design parameters are analyzed. In particular, attention is devoted to the influence of the tank geometry, through the variation of the aspect ratio, and to the impact of the source storage system size, by varying the number of desorption tanks connected in parallel. The results are presented in terms of the temporal evolution of pressure, temperature, and absolute variation of hydrogen concentration (ΔX) within the tanks. A thorough comparison on the hydrogen transfer performance is then carried out across all cases.

3.1 Sensitivity analysis on pressure ramp duration and HTF flow rate

The first set of results focuses on the effect of the pressure ramp duration. Figure 2 shows the evolution of the average hydrogen pressure in both the absorption and desorption tanks, together with the inlet pressure of the

absorption tank and the outlet pressure of the desorption tank, for different values of t_{ramp}. Figure 3 instead reports the corresponding evolution of the average temperature in the MH beds and the absolute variation of hydrogen concentration in both tanks for the two pressure ramp conditions considered. Both figures refer to the first 30 seconds of simulation, in order to provide insights on the initial transient behavior of the system.

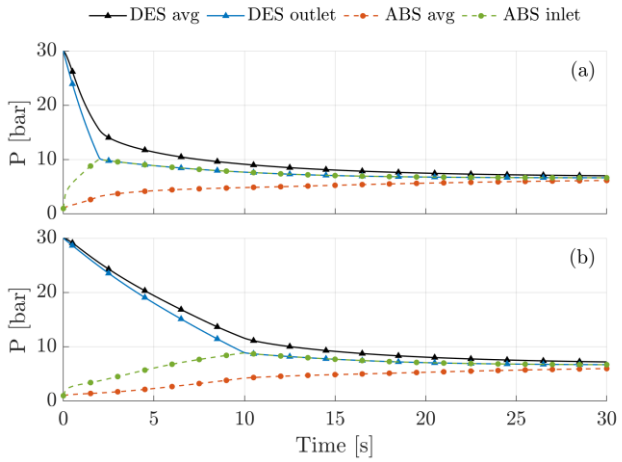

Figure 2. Case #1. Average pressure and boundary pressure in the ABS and DES tanks for (a) $t_{ramp} = 2\ s$ and (b) $t_{ramp} = 10\ s$.

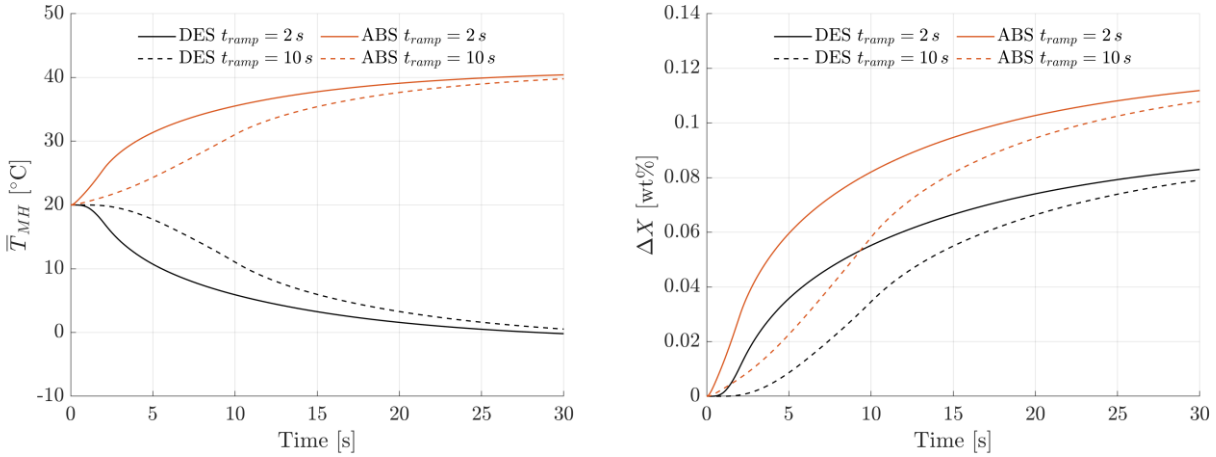

Figure 3. Case #1. Average MH temperature (left) and absolute average H_2 concentration variation (right) in the ABS and DES tanks, for $t_{ramp} = 2\ s$ and $t_{ramp} = 10\ s$.

As the valve connecting the two tanks is progressively opened, hydrogen is released from the desorption tank, leading to a gradual decrease in its pressure. At the same time, hydrogen flows toward the absorption tank, where it is taken up by the MH material, causing a corresponding increase in pressure. The temperature in the two tanks vary accordingly. When the ramp phase is completed, the inlet pressure of the absorption tank and the outlet pressure of the desorption tank become equal and subsequently evolve together, following a common trajectory dictated by the coupled absorption and desorption kinetics. A smoother evolution of the average pressure is observed for the longer ramp duration, as expected, which in turn leads to more gradual temperature and hydrogen concentration variations in both tanks. By the end of the considered time window, both the achieved temperatures and hydrogen concentration variations in the two considered cases are very close to each other, in both tanks. Overall, no significant impact of the pressure ramp duration is observed on the system behavior. However, the 10 s ramp is selected for all subsequent simulations, as it ensures a more gradual initial transition of MH thermodynamic variables, which is beneficial from a numerical standpoint. Next, Figure 4 shows the evolution of the HTF temperatures, for the two considered HTF velocity values, at the absorption tank inlet (coinciding with the desorption tank outlet) and at the absorption tank outlet (coinciding with the desorption tank inlet), together with the corresponding hydrogen concentration variation in both tanks. The results still refer to the reference configuration (Case #1) with $t_{ramp} = 10\ s$. At an HTF velocity of approximately 0.1 m/s, the temperature difference between the inlet and outlet of the two tanks is about 0.5 °C. When the HTF velocity is increased by one order of magnitude (≅1 m/s), this temperature difference is significantly reduced, becoming almost negligible. This indicates that, in the latter case, the HTF mass flow rate is sufficiently high to maintain an almost constant fluid temperature along the channel, which represents an ideal heat transfer condition. Despite these differences in thermal gradients, no appreciable variation is observed in the evolution of ΔX between the two cases, suggesting that the HTF velocity does not significantly

affect the overall hydrogen transfer performance, for the considered layout and operating conditions. That is, both velocity levels can be considered suitable for effective system operation. Nevertheless, the higher velocity of 1 m/s is selected for all subsequent simulations, as it provides overall improved performance.

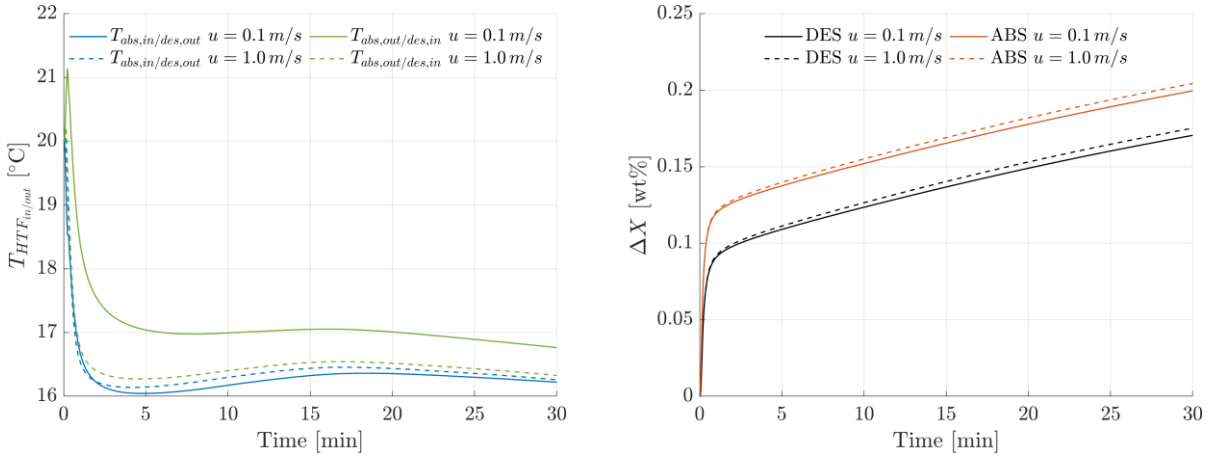

Figure 4. Case #1. HTF temperature at the ABS tank inlet (DES outlet) and at the ABS tank outlet (DES inlet), (left) and absolute average H_2 concentration variation in the ABS and DES tanks (right), for HTF velocities of 0.1 and 1 m/s.

3.2 Effect of tank layout and source storage system size

This section analyzes the combined effect of tank geometry and source system size on the hydrogen transfer performance. Table 4 summarizes the main results obtained for all the investigated cases, including: (i) the final global common pressure P^* established between the two sub-systems, (ii) the total hydrogen mass transferred to the absorption tank, and (iii) the final reacted fraction, and the maximum and final average temperatures of the MH beds in both the absorption tank and desorption tank(s).

The results clearly show that, at a fixed number of desorption tanks, increasing the aspect ratio, i.e., adopting more slender tank geometries, leads to improved hydrogen transfer performance. This is evidenced by the increase in transferred hydrogen mass (e.g., Cases 1#, #4, and #7). The underlying reason is that higher aspect ratios enhance heat transfer: slender configurations provide a larger effective heat exchange surface with the HTF and a reduced radial thickness, thus facilitating thermal transport within the MH bed. As a result, both the maximum and final temperatures in the material decrease, promoting more favorable thermodynamic conditions for absorption. This effect becomes even more pronounced as the number of desorption tanks increases. For instance, the transferred hydrogen mass increases from about 6 to 8.8 g between Cases #1 and #7, while it rises from 20.6 to 40.6 g between Cases #3 and #9. This highlights a strong coupling between geometric design and system scaling, with the benefits of improved heat transfer being amplified in larger source systems.

Table 4. Summary of: achieved global pressure, transferred mass of hydrogen, reacted fraction, and MH temperatures, for all cases.

Case ID	P^* [bar]	$m_{H_2,abs,in}$ [g]	ABS tank			DES tank(s)		
			F [-]	$\bar{T}_{MH,max}$ [°C]	$\bar{T}_{MH,end}$ [°C]	F [-]	$\bar{T}_{MH,min}$ [°C]	$\bar{T}_{MH,end}$ [°C]
1	7.26	6.0	19.5	41.0	29.0	90.3	-1.5	6.3
2	24.55	19.0	43.5	67.9	51.9	98.6	18.1	19.5
3	27.08	20.6	46.4	70.3	54.2	99.5	19.5	20.1
4	7.32	7.8	23.0	38.2	21.6	86.8	1.5	11.1
5	23.30	28.8	62.7	65.4	42.4	97.8	18.2	20.3
6	26.45	31.9	68.5	67.8	44.8	99.1	19.5	20.4
7	7.27	8.8	24.8	34.4	18.7	85.1	5.5	13.0
8	22.16	36.2	77.1	60.8	35.1	97.2	18.4	20.6
9	25.90	40.6	85.3	63.3	36.3	98.8	19.6	20.5

Concerning the effect of the number of desorption tanks, a substantial performance enhancement is observed as their number increases (e.g., Cases #1, #2, and #3). In the most favorable configuration (highest aspect ratio), the transferred hydrogen mass increases by nearly a factor of five when moving from 1 to 50 desorption tanks (Cases #7 to #9), as can also be observed from the hydrogen mass and concentration profiles reported in Figure 5. In particular, Figure 5 shows the temporal evolution of the hydrogen mass transferred into the absorption tank, distinguishing between the fraction absorbed in the solid phase ($m_{abs,a}$) and the amount present in the gaseous phase ($m_{abs,gas}$). Similarly, the figure reports the total hydrogen mass desorbed from the source system ($m_{des,d,tot}$), along with the evolution of the hydrogen mass in the gas phase within the

desorption tanks ($m_{des,gas,tot}$). It is worth noting that the variation of the gaseous hydrogen fraction remains relatively small compared to the overall mass transfer.

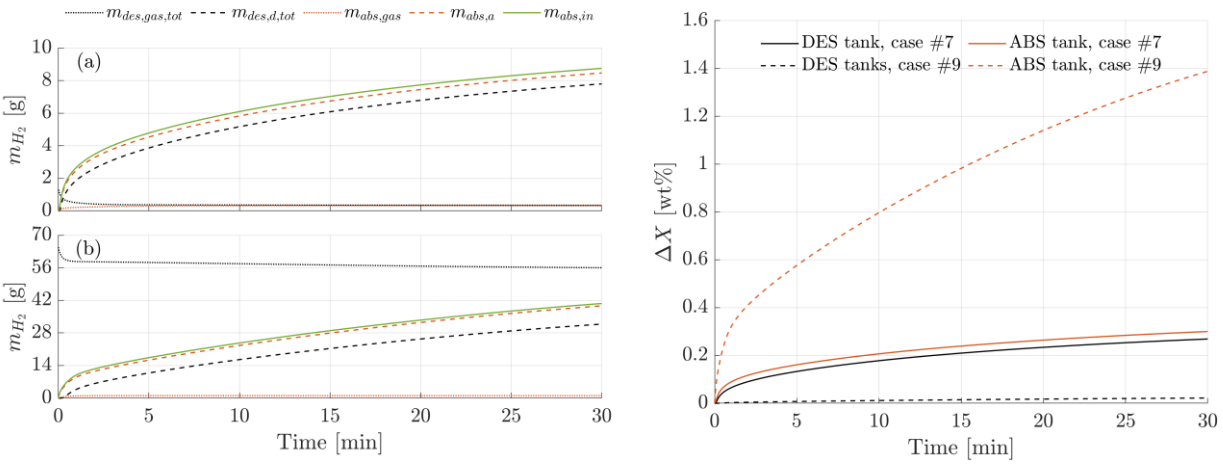

Figure 5. H_2 mass profiles for (a) Case #7 and (b) Case #9 (left), and absolute average H_2 concentration variation (right), in the absorption and desorption systems.

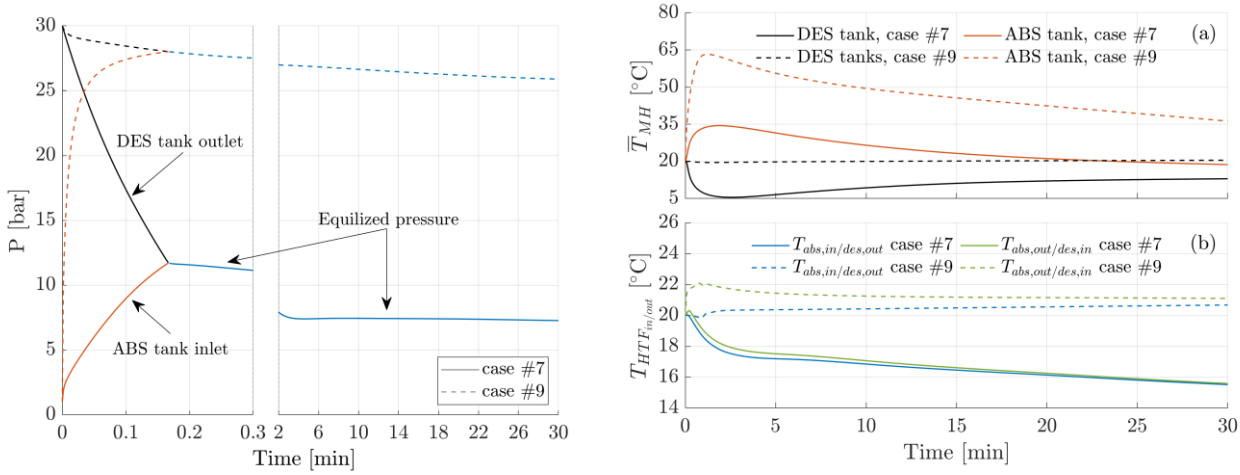

Figure 6. Local pressure (left) and average MH temperature (a) and HTF inlet/outlet temperatures (b) (right), in the absorption and desorption systems.

The observed increase in hydrogen transfer performance with the number of desorption tanks can be explained by two main factors. First, distributing the desorbed hydrogen over multiple tanks leads to a higher global pressure, which strengthens the driving force for absorption. This is clearly illustrated in Figure 6, where a comparison between Cases #7 and #9 is reported. In particular, the inlet and outlet pressures of the two sub-domains converge toward significantly different levels depending on the number of desorption tanks, reaching approximately 7 bar in Case #7 and about 26 bar in Case #9. Since only a small fraction of hydrogen is extracted from each desorption tank in the latter case, their internal pressure remains close to the initial value, allowing the global pressure to rise significantly above the absorption plateau equilibrium pressure. This condition is particularly beneficial, as it enables sustained absorption over a wide range of hydrogen concentration. Second, the heat load associated with desorption is distributed among multiple tanks, meaning that each unit experiences only a limited thermal demand. As a consequence, the HTF, entering at near-ambient temperature, is more effective in maintaining favorable thermal conditions. This is reflected in the desorption tanks, whose average temperature remains close to the initial ambient value (≈20 °C) at the end of the 30 minute operation for configurations with 20 or 50 tanks. In the most favorable case (Case #9), the temperature of the desorption tanks remains nearly constant throughout the process. In contrast, the temperature in the absorption tank increases with the number of desorption tanks, due to the significantly larger amount of hydrogen being absorbed. Nevertheless, even in the most demanding case (Case #9), the maximum average temperature reaches approximately 64 °C, which remains relatively moderate (Figure 6). Under these conditions, about 41 g of hydrogen, corresponding to roughly 77% of the nominal tank capacity, is transferred within 30 minutes, confirming the effectiveness of the proposed thermally coupled configuration. Figure 6 also reports the evolution of the HTF temperature at the inlet and outlet sections of the tanks, comparing Cases #7 and #9. The results further highlight the different thermal behavior of the system: in Case #9 (50 desorption tanks), the HTF temperature remains within a narrow range between approximately 20 °C

and 22 °C, indicating near-isothermal conditions. In contrast, in Case #7 (single desorption tank), the HTF temperature decreases down to about 16 °C. This behavior is due to the larger relative impact of the endothermic desorption process, which dominates over absorption and drives the system toward lower temperatures compared to the initial condition.
Overall, the results clearly highlight the benefit of scaling the source storage system. Increasing the number of desorption tanks enhances both the thermodynamic driving force for hydrogen uptake in the receiver tank and the thermal management capabilities, leading to significantly improved hydrogen transfer performance while maintaining favorable operating temperatures.

4. Conclusion

Hydrogen absorption and desorption in MHs involve significant thermal effects, requiring substantial heat removal and supply during the respective processes, which makes thermal management a key challenge. In addition, there is a need of achieving rapid and efficient refueling operation for MH tanks. In this work, a thermally coupled system operating under self-sustaining conditions has been investigated, where the endothermic heat associated with desorption drives the exothermic absorption process, and viceversa, through a closed-loop HTF. In the proposed approach, hydrogen transfer continues as long as a driving force exists between the two sub-systems, progressively evolving toward a condition in which the equilibrium pressures of both absorption and desorption systems converge toward the common global pressure. This coupled MH tank configuration mitigates the need for external heating and cooling, resulting in high overall thermal efficiency. The results show that scaling the source system and optimizing tank geometry significantly enhance hydrogen transfer performance. In particular, when a large number of desorption tanks is considered, the global system pressure becomes significantly higher than the plateau equilibrium pressure of the absorption process. As a consequence, hydrogen absorption is promoted and the hydrogen transfer proceeds effectively over a wide range of hydrogen concentrations levels.

References

[1] B. Reda, *et al*., “Green hydrogen as a source of renewable energy: a step towards sustainability, an overview”, Environ. Dev. Sustain. 27, 29213–29233 (2025), https://doi.org/10.1007/s10668-024-04892-z

[2] A.S. Mehr, A.D. Phillips, M.P. Brandon, M.T. Pryce, J.G. Carton, ”Recent challenges and development of technical and technoeconomic aspects for hydrogen storage, insights at different scales; A state of art review”, Int. J. Hydrog. Energy 70, 786-815 (2024), https://doi.org/10.1016/j.ijhydene.2024.05.182

[3] J. Zheng, X. Liu, P. Xu, *et al*., “Development of high pressure gaseous hydrogen storage technologies”, Int. J. Hydrog. Energy 37, 1048–1057 (2012), https://doi.org/10.1016/j.ijhydene.2011.02.125

[4] M. Aziz, “Liquid Hydrogen: A Review on Liquefaction, Storage, Transportation, and Safety”, Energies 14(18), 5917 (2021), https://doi.org/10.3390/en14185917

[5] M. Simanullang, L. Prost, “Nanomaterials for on-board solid-state hydrogen storage applications”, Int. J. Hydrog. Energy 47, 29808–29846 (2022), https://doi.org/10.1016/j.ijhydene.2022.06.301

[6] G. Scarpati, E. Frasci, G. Di Ilio, E. Jannelli, “A comprehensive review on metal hydrides-based hydrogen storage systems for mobile applications,” J. Energy Storage 102, 113934 (2024), https://doi.org/10.1016/j.est.2024.113934

[7] C. Drawer, J. Lange , M. Kaltschmitt, "Metal hydrides for hydrogen storage – Identification and evaluation of stationary and transportation applications", J. Energy Storage 77, 109988 (2024), https://doi.org/10.1016/j.est.2023.109988

[8] L. Schlapbach, A. Züttel, “Hydrogen-storage materials for mobile applications,” Nature 414, 353–358 (2001), https://doi.org/10.1038/35104634

[9] M. Afzal, R. Mane, P. Sharma, “Heat transfer techniques in metal hydride hydrogen storage: A review,” Int. J. Hydrog. Energy 42, 30661–30682 (2017), https://doi.org/10.1016/j.ijhydene.2017.10.166

[10] S. Parashar, A. More, J.S. Prasad, P. Muthukumar, A.K. Soti, “Experimental study on charging and discharging characteristics of copper finned metal hydride reactor for stationary hydrogen storage applications”, J. Energy Storage 86, 111144 (2024), https://doi.org/10.1016/j.est.2024.111144

[11] G. Scarpati, G. Di Ilio, E. Jannelli, “Design and analysis of an energy-efficient, large scale metal hydride hydrogen storage system using an extended multi-physics numerical model,” Appl. Energy 409, 127452 (2026), https://doi.org/10.1016/j.apenergy.2026.127452

[12] L. Tong, *et. al*, “Complete and reduced models for metal hydride reactor with coiled-tube heat exchanger”, International J. Hydrogen Energy 44, 15907-15916 (2019), https://doi.org/10.1016/j.ijhydene.2018.07.102

[13] F. Askri, M. Ben Salah, A. Jemni, S. Ben Nasrallah, “Optimization of hydrogen storage in metal-hydride tanks”, Int. J. Hydrog. Energy 34, 897–905 (2009), https://doi.org/10.1016/j.ijhydene.2008.11.021
[14] S. Gupta, V.K. Sharma, “Design and analysis of metal hydride reactor embedded with internal copper fins and external water”, Int. J. Energy Res. 45, 1836–56 (2021), https://doi.org/10.1002/er.5859
[15] S.N. Nyamsi, I. Tolj, “Metal hydride reactors and phase change materials: enhancing energy storage for medium-high power vehicles”, J. Energy Storage 104, 114545 (2024), https://doi.org/10.1016/j.est.2024.114545
[16] A. Wimmer, M. Kordel, M. Linder, I. Bürger, “High performance reactor of a metal hydride based cooling system for air-conditioning of fuel cell electric vehicles”, Appl. Energy 391, 125911 (2025), https://doi.org/10.1016/j.apenergy.2025.125911
[17] A. Wimmer, M. Linder, I. Bürger, ”Metal hydride-based cooling system for fuel cell electric vehicles: achieving a temperature lift of 40 K”, Appl. Energy 398, 126396 (2025), https://doi.org/10.1016/j.apenergy.2025.126396
[18] Y. Ye, *et al.*, “Performance optimization of metal hydride hydrogen storage reactors based on PCM thermal management”, Appl. Energy 338, 120923 (2023), https://doi.org/10.1016/j.apenergy.2023.120923
[19] M. Maggini, A.L. Facci, G. Falcucci, S. Ubertini, “Increasing the Metal-Hydride Power Density Using Phase-Change Materials, Advanced Thermal Supports, and Expanded Graphite Nano-Particles”, Energies 19, 185 (2026), https://doi.org/10.3390/en19010185
[20] P. Di Giorgio, G. Di Ilio, E. Jannelli, F.V. Conte, “Innovative battery thermal management system based on hydrogen storage in metal hydrides for fuel cell hybrid electric vehicles”, Appl. Energy 315, 118935 (2022), https://doi.org/10.1016/j.apenergy.2022.118935
[21] P. Di Giorgio, G. Di Ilio, G. Scarpati, G. Erme, E. Simeoni, E. Jannelli, “Design of a hydrogen-powered bicycle for sustainable mobility”, E3S Web Conferences 334, 06012 (2022), https://doi.org/10.1051/e3sconf/202233406012
[22] P. Di Giorgio, G. Scarpati, G. Di Ilio, I. Arsie, E. Jannelli, “Development of a plug-in fuel cell electric scooter with thermally integrated storage system based on hydrogen in metal hydrides and battery pack”, E3S Web Conferences 334, 06013 (2022), https://doi.org/10.1051/e3sconf/202233406013
[23] P. Di Giorgio, G. Di Ilio, E. Jannelli, F.V. Conte, “Numerical analysis of an energy storage system based on a metal hydride hydrogen tank and a lithium-ion battery pack for a plug-in fuel cell electric scooter”, Int. J. Hydrog. Energy 48, 3552–65 (2023), https://doi.org/10.1016/j.ijhydene.2022.10.205
[24] P. Di Giorgio, G. Di Ilio, G. Scarpati, A. Altomonte, E. Jannelli, “Thermally integrated energy storage system for hybrid fuel cell electric bike: an experimental study”, Int. J. Hydrog. Energy 48, 20914-20922 (2023), https://doi.org/10.1016/j.ijhydene.2022.10.043
[25] G. Capurso, B. Schiavo, *et al.*, “Development of a modular room-temperature hydride storage system for vehicular applications”, Applied Physics A 122, 236 (2016), https://doi.org/10.1007/s00339-016-9771-x
[26] J.A. Puszkiel, A.M. Neves, *et al*. “On the hydrogen storage properties and life cycle evaluation of a room temperature hydride for scale-up applications: the case of an AB2-alloy”, Int. J. Hydrog. Energy 118, 482–499 (2025), https://doi.org/10.1016/j.ijhydene.2025.03.161
[27] V. M. Skripnyuk, M. Ron, “Hydrogen desorption kinetics in intermetallic compounds C2, C51 and C52 with Laves phase structure,” Int. J. Hydrog. Energy 28, 303–309 (2003), https://doi.org/10.1016/S0360-3199(02)00081-2
[28] M. Ron “The normalized pressure dependence method for the evaluation of kinetic rates of metal hydride formation/decomposition”, J. Alloys Compd. 283, 178–191 (1999), https://doi.org/10.1016/S0925-8388(98)00859-7
[29] K. Herbrig, L. Rontzsch, *et al.*, “Hydrogen storage systems based on hydride-graphite composites: computer simulation and experimental validation”, Int. J. Hydrog. Energy 38, 7026–7036 (2013), https://doi.org/10.1016/j.ijhydene.2013.03.104
[30] D.O. Dunikov, D.V. Blinov, *et al*. “Permeability of a deformable metal hydride bed during hydrogen absorption”, Int. J. Hydrog. Energy 51, 375-387 (2024), https://doi.org/10.1016/j.ijhydene.2023.05.224
[31] D.W. Sun, S.J. Deng, “Theoretical descriptions and experimental measurements on the effective thermal conductivity in metal hydride powder beds”, J. Less-Common Metals 160, 387–395 (1990), https://doi.org/10.1016/0022-5088(90)90397-3